# Synthesis of Solar-Sensitive ZnO Photocatalysts Using Microwave Plasma for Effective Degradation of Phenols and Antibiotics

Arsen Muslimov * , Sergey Antipov , Makhach Gadzhiev , Anna Ulyankina , Vladimir Kanevsky

Posted Date: 11 October 2023

doi: 10.20944/preprints202310.0682.v1

Keywords: photocatalytic activity; microwave plasma; zinc oxide; antibiotic; dinitrophenol; solar radiation

*Article*

# Synthesis of Solar-Sensitive ZnO Photocatalysts Using Microwave Plasma for Effective Degradation of Phenols and Antibiotics

**Arsen Muslimov [1,*], Sergei Antipov [2], Makhach Gadzhiev [2], Anna Ulyankina [3] and Vladimir Kanevsky [1]**

[1] Federal Scientific Research Centre "Crystallography and Photonics" of Russian Academy of Sciences, Shubnikov Institute of Crystallography, 119333 Moscow, Russia
[2] Joint Institute for High Temperatures, Russian Academy of Sciences, 125412 Moscow, Russia
[3] Platov South-Russian State Polytechnic University (NPI) Novocherkassk, Russian Federation
* Correspondence: amuslimov@mail.ru

**Abstract:** The presented work studies the processes of synthesis of nitrogen-containing structures of ZnO using atmospheric pressure microwave nitrogen plasma and investigates their photocatalytic activity in the processes of degradation of 2,4-dinitrophenol and the antibiotic ciprofloxacin when irradiated with sunlight. The work proposes an effective method for formation of photosensitive ZnO powders. Due to the features of plasma treatment in the open atmosphere of zinc metal microparticles, ZnO structures are formed with sizes from hundreds of nanometers to several micrometers with various micromorphologies. High photoactivity was demonstrated (rate constants 0.036 $min^{-1}$ and 0.051 $min^{-1}$) of synthesized ZnO structures during photo-degradation of 2,4-dinitrophenol and ciprofloxacin, respectively, when exposed to solar radiation. Photo-active structures of ZnO synthesized using microwave nitrogen plasma can find application in processes of mineralization of toxic organic compounds.

**Keywords:** photocatalytic activity; microwave plasma; zinc oxide; antibiotic; dinitrophenol; solar radiation

## 1. Introduction

All over the world today there is a shortage of clean water due to rapid population growth, environmental degradation, uncontrolled disposals from industrial enterprises and the widespread introduction of chemical technologies in agriculture. Despite the widespread construction of modern treatment facilities, it is not possible to achieve complete wastewater treatment. This is due to the presence of difficult-to-oxidize organic pollutants, the most common of which are phenol-containing substances and antibiotics. Traditional treatment methods include mainly biological treatment and a number of physicochemical methods such as adsorption, ion exchange and reverse osmosis. The disadvantages of these methods include the non-destructive nature of cleaning, high energy and operating costs, low efficiency and the generation of large amounts of waste. In recent years, environmentally friendly and energy-efficient advanced oxidation technologies have been actively developed, among which photo-catalysis (PC) occupies an important place [1,2]. An important advantage of PC is the possibility of oxidation at relatively low concentrations of pollutants [3], which is important for the mineralization of toxic organic pollutants with low maximum permissible concentrations. The efficiency of PC is determined by the efficiency of formation and separation of photo-charges. For a long time, the main photo-catalyst produced on an industrial scale was titanium dioxide ($TiO_2$) from Degussa (P-25) [4]. The disadvantage of $TiO_2$ is its significant band gap (Eg = 3.2 eV) and its maximum photo-catalytic activity when irradiated with ultraviolet (UV) light. Ultraviolet radiation takes up only 5-7% of solar radiation. At the same time, visible radiation makes up about

 doi:10.20944/preprints202310.0682.v1



45% and the search for photo-catalysts active in the visible region is very relevant. A huge number of works are devoted to heterostructural and composite photo-catalysts exhibiting activity in the visible region [5–10]. Despite individual studies demonstrating the effectiveness of hybrid photo-catalysts, the traditionally used $TiO_2$ still remains the most popular. This is due to the lack of economically accessible technology for mass production of hybrid photo-catalysts. As an alternative to $TiO_2$, ZnO [11,12], which is not inferior in efficiency and availability, has recently been actively studied. Despite the similarity of the band gap of ZnO (3.37 eV) with $TiO_2$ (3.2 eV), a distinctive feature of the band structure of ZnO is the presence of isolated energy levels in the band gap associated with point defects, mainly oxygen vacancies [13]. With a significant increase in the concentration of vacancies, photosensitivity can expand into the visible region of the spectrum. An additional source of levels in the forbidden zone are dislocations. The band structure is distorted around the dislocation core and a level is introduced closer to the center of the band gap. In n-type crystals, which include ZnO, dislocations can capture electrons and prevent their recombination. The highest concentration of defects is observed in crystals synthesized under conditions that are far from ideal: high saturation, unstable temperature gradient, chaotic influx of atoms. Such conditions can be created using plasma synthesis of metal oxide structures [14]. Plasma synthesis using gas-discharge plasma is not only energy efficient, but also has a high productivity. Of greatest interest is the microwave (MW) discharge of atmospheric pressure, which has a much higher charge density and, as a consequence, greater reactivity compared to other discharges at the same power. Note also that in some types of atmospheric pressure discharges (corona, spark and arc), the plasma is “contaminated” by the material of the internal discharge electrodes. This can be avoided by investing energy in a microwave discharge excited in discharge chambers (for example, dielectric tubes) in the absence of direct contact with metal electrodes. This property is of fundamental importance for creating high-purity plasma. It should be noted that the possibility of using microwave plasma for the synthesis of photocatalytically active ZnO tetrapods was previously studied in [15]. However, the authors pay attention only to plasma regions in which the conditions for the formation of ZnO tetrapods are realized. This approach generally limits the performance of the photoactive ZnO catalyst. It seems to us that loading zinc metal powder directly into the gas transportation system is an important technological solution. Thus, the residence time of zinc metal in the plasma increases. Taking into account the plasma temperature of 5000-6000 K, one can expect instantaneous evaporation of zinc and the formation of individual ZnO elements with a wide range of sizes and different micromorphologies. It should be noted that micron-sized particles injected into a gas-discharge plasma become centers of recombination of plasma electrons and ions (sometimes a source of electrons owing to thermo-, photo-, and secondary electron emissions) and acquire a negative electric charge because of the greater mobility of electrons. In this case, the particle charge can reach significant values of up to $10^3$-$10^5$ electron charges [16,17]. Owing to electrostatic interaction, particles of the same charge sign experience mutual Coulomb repulsion, which prevents them from sticking together and forming agglomerates. As a result, the form of individual ZnO elements with a large variation in size and different micromorphology with a developed surface can be expected. In order to enhance the photosensitivity of ZnO powder in the visible region, one can resort to nitridation of ZnO [18]. For this purpose, it is possible to use nitrogen as a buffer plasma-forming gas.

In the presented work, the processes of synthesis of nitrogen-containing ZnO structures using microwave plasma were studied and their photocatalytic activity in the processes of degradation of 2,4-dinitrophenol and the antibiotic ciprofloxacin under irradiation with sunlight was investigated.

## 2. Materials and Methods

For the experiment, zinc powders (99.98% purity) 30-40 μm mean particle size provided by OCHV, Russia, were used. The waveguide microwave atmospheric-pressure plasmatron was used for ZnO plasma synthesis. The plasma synthesis technique and its features are discussed in detail in the next section. For microscopic studies, the JCM-6000 (JEOL, Tokyo, Japan) desktop scanning electron microscope (SEM) equipped with equipped with an energy dispersive X-ray (EDX) microanalyzer were used. X-ray studies were carried out on an X’PERTPRO diffractometer

 doi:10.20944/preprints202310.0682.v1



(PANalytical, Almelo, Netherlands) in the Bragg–Brentano "reflection" geometry using $CuK_\alpha$ radiation ($\lambda$ = 1.54 Å) with a Ni β-filter. Previously, the powder was thoroughly rubbed. X-ray photoelectron spectroscopy (XPS) using the SPECS spectrometer (Specs, Berlin, Germany) equipped with Al and Mg anodes was used to determine the chemical composition of the surface layer and to measurement valence band of the samples. The spectrometer is metrologically verified. In this work, we used Al anode excitation. The anode material was chosen in such a way that the useful signal did not overlap with the Auger lines. The spectra were recorded in the binding energy range from 0 to 1200 eV. The binding energies were calibrated over the C-C line of the C1s spectrum ($E_q$ = 284.6 eV). The etching was carried out with argon ions with energy of 4 keV for 2 minutes. To determine the band gap by UV/VIS spectroscopy, a spectrometric complex based on the MDR-41 monochromator (NPO Spektr, Russia) was used. The material powder was poured onto a special holder and compacted thoroughly. Diffuse reflectance spectra were taken in the wavelength range 200 to 500 nm.

To study the photo-catalytic activity of the synthesized materials, ZnO powder (25 mg) was placed in aqueous solutions of 2,4-dinitrophenol (DNP) and ciprofloxacin (CIP) (volume 50 ml with a concentration of 5 mg/l), stirred in the dark for 30 min, then the suspension was irradiated light with constant stirring. A solar radiation simulator (xenon lamp, 100 mW/cm2) was used as a light source. The DNP concentration was determined spectrophotometrically based on the absorption maximum at 358 nm (Shimadzu UV-1800 spectrophotometer).

## 3. Results

### *3.1. Features of Plasma Synthesis of Oxide Powders*

We used the microwave plasmatron developed on the base on a 2.45-GHz magnetron with an output power of 1.1 kW. Unlike microwave plasmatrons of a "classical" design, our plasmatron is built using simplified scheme "power supply - magnetron - waveguide - gas-discharge device - load". The WR-340 waveguide (Figure 1) was made from a stainless-steel standard rectangular profile 100×500×2 mm. At the end of the waveguide there is a resonant water load. In the middle of the wide walls of the waveguide central part two pipe nozzles are welded coaxially for a gas discharge device input. A dielectric (quartz) tube with an internal diameter of 3 cm was placed through the nozzles normal to the wide wall of the waveguide. A volumetric atmospheric-pressure stationary discharge was excited in the tube by microwaves inside the waveguide, operating in the $H_{10}$ mode. Thus, the tube acts as a plasma-chemical reactor in which microwave plasma is generated and through which the plasma-forming gas flows along with the dispersed particles being processed. High purity nitrogen (99.998%) was used as a plasma-forming gas, which was introduced into the tube at a flow rate of 1-10 l/min.

To operate the magnetron, a high-voltage power supply circuit, which allows receiving up to 3 kW of continuous output power from the magnetron, was used. The microwave discharge in a continuous wave (CW) regime can be obtained with the help of 'seed' ionization using a thin metal wire tip brought into the tube.

 doi:10.20944/preprints202310.0682.v1



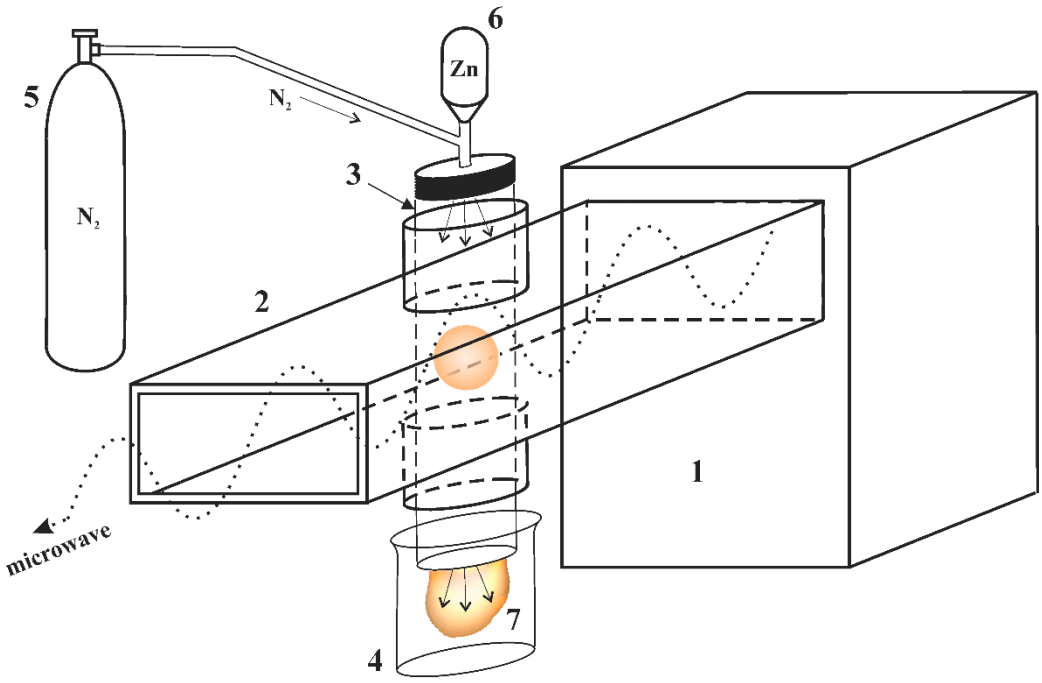


**Figure 1.** Scheme of the experimental setup with microwave plasmatron: 1 – microwave unit with 2.45-GHz magnetron, 2 – rectangular waveguide, 3 – quartz tube, 4 – quartz cup, 5 – $N_2$ gas cylinder, 6 – container with Zn powder, 7 – microwave plasma flame with synthesized ZnO.

To mix the powder with the working gas, a simple transparent sealed container with visual control was used. Zinc powder with particle sizes of 30-40 μm was poured out from the container into the discharge tube from the gas supply side and passed through the microwave discharge region inside the waveguide. Next, the particles of the treated zinc powder were collected through the open end of the discharge tube into a quartz cup.

To organize microparticles injection into a discharge, several features of a microwave discharge at atmospheric pressure should be considered. Commonly, to maintain the stability of the discharge and isolate it from the walls of the discharge tube various schemes for "swirling" the gas jet are used. However, in this case, when solid dispersed particles are injected into the gas flow, they are centrifugally ejected from the central region onto the tube wall. To reduce the deposition of the powder onto the walls, plasma-forming gas was introduced almost without swirling.

Let us describe the advantages of the microwave plasma method we are developing for the synthesis of ZnO structures. It is known that in some types of atmospheric-pressure discharges (corona, spark and arc), the plasma is inevitably "contaminated" by the material of the internal discharge electrodes. This can be avoided using dielectric tubes crossing the waveguide. Since in this case there are no electrodes or direct contact of the plasma with the conductive parts of the gas-discharge device, this type of the discharge is called "electrodeless". This characteristic is of fundamental importance for the generation of high-purity plasma (without impurities of electrode material).

It should be emphasized that when it comes to the efficiency of a discharge device, it is necessary to consider the materials of all its internal elements that may be exposed to plasma particles. Energy losses due to interaction with the electrode metal, even if this does not lead to noticeable contamination of the processed materials, in any case, reduces the efficiency of the reactor. The use of a microwave plasmatron for material plasma modification makes it possible to combine the advantages of a pure electrodeless discharge with the convenience of electromagnetic energy supply through waveguides [19].

It should also be noted that placing the tube in the branch nozzles of the waveguide perpendicular to its wide walls makes it possible to use tubes of larger diameter. This makes it

 doi:10.20944/preprints202310.0682.v1



possible to maintain discharge stability when processing a large amount of material and thus increase the productivity of the method.

In our method the powder is injected into the discharge tube from the side of the gas supply. This led to intensive plasma treatment since the particles pass both through the discharge zone in the waveguide and the region of the plasma jet (flame) behind the exit from the branch pipes. Without particles, a microwave plasmatron of a "classical" electrodeless design generate an atmospheric-pressure plasma with a gas temperature of several thousand degrees. Namely, from the results of spectral diagnostics of a microwave discharge plasma in a nitrogen flow, it is known that the gas temperature on the axis of the discharge tube is 5000-6000 K, while the concentration and temperature of electrons in the plasma are $10^{13}$ $cm^{-3}$ and 1 eV, respectively [20].

### *3.2. ZnO Powder Characterization*

According to electron microscopy data (Figure 2a) a morphologically heterogeneous crystalline precipitate is formed during synthesis. Among the individual elements of the precipitate, thetrapods, hexagonal rods can be observed. The structures range in size from hundreds of nanometers to a few micrometers. According to EDX (Table 1), the composition of the ZnO powder contained, in addition to the main components of zinc and oxygen, an atomic fraction of nitrogen of the order of 4%, which confirms the nitridization of the precipitate. The observed excess oxygen content is associated with water vapors and oxygen absorbed by the surface of ZnO structures as well as contained in the pores of ZnO powder. Diffraction reflections on the X-ray diffraction spectrum of oxidized zinc microstructures correspond to the hexagonal wurtzite structure of ZnO [JCPDS No. 79-0205]. The most intense reflections are observed at 31.68 °, 34.35 ° and 36.16 °, corresponding to reflections from planes (100), (002) and (101) ZnO with little displacement towards smaller angles. Displacement may be due to an increase in the lattice parameter ZnO due to partial substitution of oxygen with nitrogen. Since the radius of nitrogen (1.46 Å) is greater than oxygen (1.38 Å), replacing oxygen with nitrogen in the ZnO lattice can cause it to deform. A similar effect was observed in [21]. According to XPS date (calculation was carried out for the spectra of Zn2p, O1s and C1s) calculated the concentrations of the main components of the powders (Table 2). It can be seen that the powder composition according to XPS was different from that obtained according to EDX (Table 1). The Zn-to-O atomic ratio, in this case, is closer to the stoichiometric value, however, there is an excess of zinc. For qualitative XPS analysis, the surface of the samples is previously etched, which results in surface cleaning. The excess of zinc found in the measurements is associated with a feature of the thermodynamically stable wurtzite phase of ZnO, in which oxygen vacancies and interstitial zinc are always present. These types of defects determine the electronic conductivity type ZnO. The presence of carbon (peak 285 eV corresponding to the C-O bond) is associated with hydrocarbon contamination of the surface, which is difficult to get rid of. Of particular note is the absence of nitrogen in the surface layer, which was previously evident in the EDX data.

**Table 1.** Concentrations (in %) of the main components of ZnO powder before photocatalysis according to EDX data.

| Element | Zn | O | N |
|---|---|---|---|
| Quantity,% | 27.56 | 68.32 | 4.12 |

**Table 2.** Concentrations (in %) of the main components of ZnO powder before and after photocatalysis according to XPS data.

| Sample | Zn | O | C | N |
|---|---|---|---|---|
| Initial | 49.6 | 40.8 | 9.6 | 0 |
| After photocatalysis | 49.5 | 41.3 | 9.2 | 0 |

 doi:10.20944/preprints202310.0682.v1



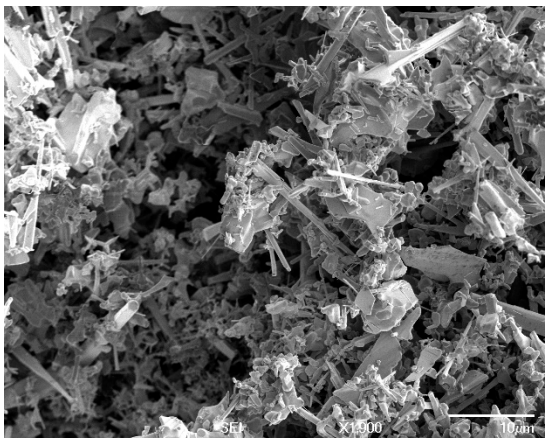


(a)

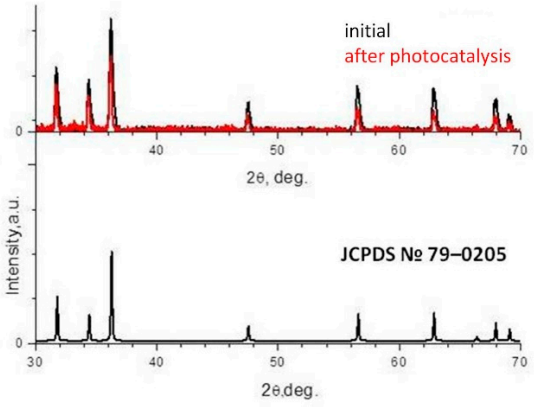


(b)

**Figure 2.** SEM images (**a**) and X-ray diffraction pattern (**b**) of ZnO powder. Scale bar: 10 μm.

The melting and evaporation temperatures of zinc are 419.5 °C and 907 °C, respectively. As the particle size decreases, their thermodynamic characteristics change, the melting and evaporation temperatures decrease. Under microwave discharge conditions, the gas temperature without particles is about 5000-6000 K. Given the decrease in particle size after plasma treatment and their large size difference (Figure 2a), evaporation of Zn microparticles at the initial stage can be assumed. This assumption is supported by the presence of ZnO sharp structures, the growth of which is determined exclusively by zinc pairs. As noted above, micron-sized dispersed particles acquire a negative electrical charge upon entering the discharge plasma. Electrostatic repulsion of microparticles prevents their agglomeration. As a result, we observe a large variation in particle size and shape after plasma treatment. Zinc atoms enters a gaseous phase and reacts with active ionized nitrogen and oxygen diffusing from the open end of the quartz tube. If nitridization processes prevail at the initial stage. Oxidation processes prevail as the particles move to the open end of the tube. Zinc nitride phases have low stability at high temperatures in the presence of oxygen. It can be assumed that at the final stage there is a substitution of nitrogen atoms with oxygen atoms in the ZnO lattice in the direction from the surface deep into the sample. In addition, the enthalpy of ZnO formation is -350 kJ/mol and energy is released during zinc oxidation, which additionally heats up the plasma. As a result, the distribution of temperature and other thermodynamic plasma parameters may be heterogeneous and a variety of ZnO forms is also associated with this. In addition, according to XRD (Figure 2 b), there is no zinc metal in the synthesized ZnO powder. The presence of an oxide film allows complete oxidation of particles even at temperatures above the melting point of zinc [22]: diffusion of oxygen through the oxide layer limiting liquid zinc in the central part of the particles.

### *3.3. Photocatalytic Properties of ZnO Powder*

The photodegradation of DNP and CIP was evaluated under simulated solar light. Figure 3a,b represents absorption spectra of unirradiated (0 min) and irradiated DNP (Figure 3a) and CIP (Figure 3b) for 2, 5, 10, 20, 30, 40, and 60 min. The observed decrease in the maximum absorbance peaks is

 doi:10.20944/preprints202310.0682.v1



due to the photocatalytic removal of the organic pollutants. Degradation of most organic compounds by photocatalysis may be described using a pseudo-first-order kinetic model for reactions that occur at the solid-liquid interface [23]. The ln ($C/C_0$) graph against time producing a linear line verifies that the reaction towards DNP and CIP follows the pseudo-first-order kinetic model. The apparent first-order rate constants ($k_{app}$) were 0.036 and 0.051 $min^{-1}$ for DNP and CIP respectively. The results of this study are compared to those of similar papers that investigated the photodegradation of DNP and CIP (Table 3).

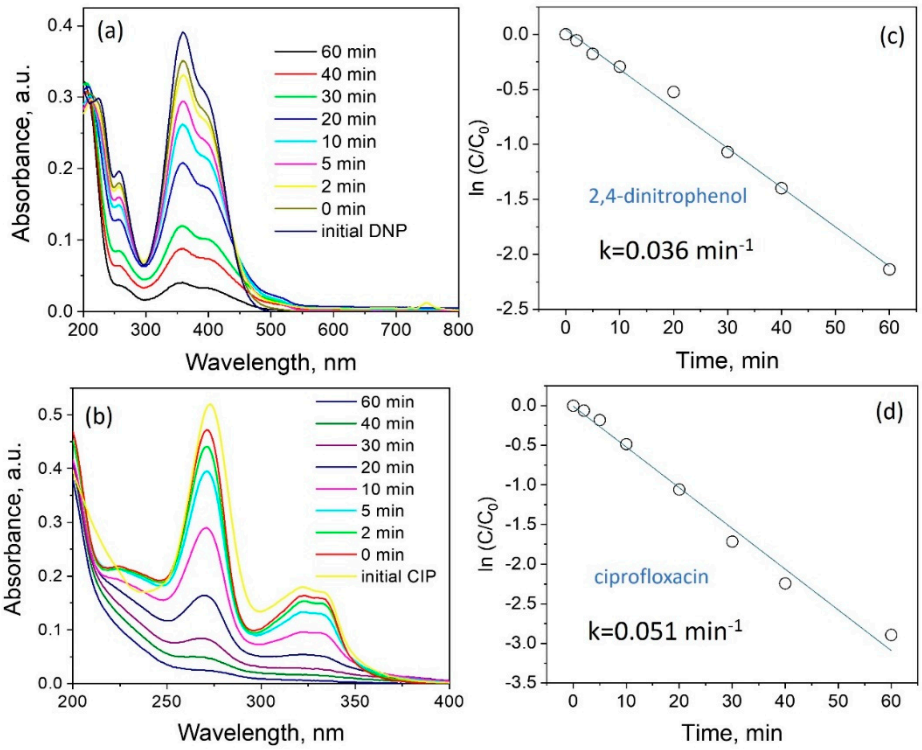


**Figure 3.** Photocatalytic performance of the synthesized ZnO powder: Absorption spectra of DNP (**a**) and CIP (**b**) photodegradation under simulated solar light; kinetic linear fitting curves for DNP (**c**) and CIP (**d**) and corresponding apparent rate constants.

The reason for the high photoactivity of ZnO structures may be several. First of all, this may be due to a structural factor. It was found [29] that nanorods have the greatest photocatalytic activity and this is associated with a high proportion of [100]-texture. According to [30,31], in the plane (100) the lowest energy of formation of defects, in particular oxygen vacancies. According to XRD (Figure 2b), the ratio I100/I001 ~ 1.27. Taking into account the large number of rod-like [001] - structures of ZnO (Figure 2a), the value of the ratio 1.27 indicates the presence of a high fraction of [100] - texture in the ZnO powder.

 doi:10.20944/preprints202310.0682.v1



**Table 3.** Comparison of some of the recent literature reports on the photocatalytic degradation of CIP and DNP by various photocatalysts with our study.

| Photocatalyst | Pollutant | Catalyst dosage ($g\ L^{-1}$) | Pollutant concentration | Light source | $k_{app}$, ($10^{-3}$ $min^{-1}$) | Reference |
|---|---|---|---|---|---|---|
| ZnO/g-$C_3N_4$ | CIP | 0.5 | 5 mg $L^{-1}$ | a 32 W compact fluorescent bulb | 24 | 24 |
| ZnO nanoparticles | CIP | 0.6 | 12 mg $L^{-1}$ | Natural sunlight, 221 $W/m^2$ | 13 | 25 |
| $TiO_2$/$SnO_2$ nanocomposite | CIP | 0.5 | 5 mg $L^{-1}$ | three UVC lamps with 35 W (253 nm) | 28.2 | 26 |
| carbon-nano-onion-functionalized ZnO tetrapods | DNP | 2 | 0.1 mM | a 60 W tungsten bulb | 18.34 | 27 |
| Commercial P25 | DNP | 2 | 5 μM | 266 $W/m^2$ Hg lamp | 32 | 28 |
| ZnO powder (microparticles) | CIP | 0.5 | 5 mg $L^{-1}$ | 500 W Xenon lamp | 51 | This work |
| | DNP | 0.5 | 5 mg $L^{-1}$ | 500 W Xenon lamp | 36 | This work |

The next important factor is the adhesion levels of charge carriers in the ZnO band gap, which are associated with defects. Adhesion levels inhibit recombination of charge carriers and enhance photocatalytic activity. To determine the energy zone structure of the ZnO powder, XPS valence band spectra was obtained and the band gap was determined (Figure 4). The presence of energy state density near Fermi energy can be seen. These levels expand the photosensitivity of ZnO to the visible area. The $VB_{max}$ energy was estimated to be 2.3 eV. Based on this, $CB_{min}$ was estimated to be -0.9 eV. The levels in the band gap are mainly associated with oxygen vacancies and interstitial zinc [32]. This correlates with the structural features of ZnO powder and their effect on photocatalytic properties. As can be seen, the presence of nitrogen in the volume of ZnO structures does not lead to a narrowing of the band gap, however, energy levels associated with the nitrogen mixture in the band gap are present. For example, the energy state (0.3-0.4) eV below the bottom of the conduction zone is associated with the $V_O$-N defect complex [33]. There is also data on the acceptor level N2p above the valence zone by 0.76 eV [18].

 doi:10.20944/preprints202310.0682.v1



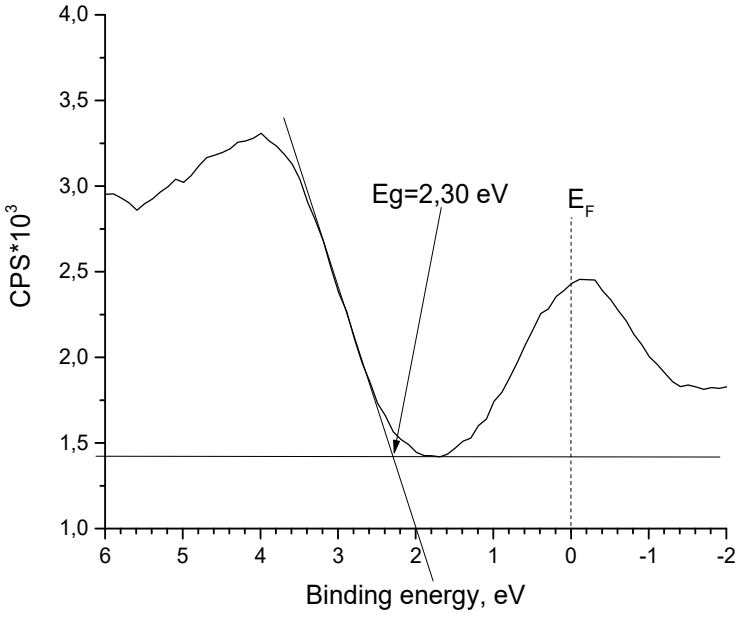


(a)

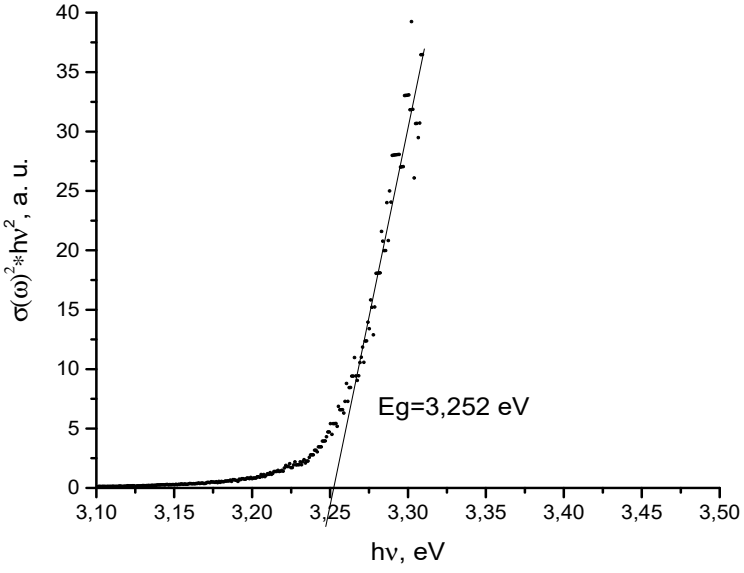


(b)

**Figure 4.** XPS valence band spectra (**a**) and Tauc's plots for the energy band gap (**b**) of ZnO powder.

An important characteristic of the photocatalyst is the preservation of structural-phase properties, composition, surface state. These characteristics affect the reproducibility of results in processes of photocatalytic degradation of organic pollutants. Samples of ZnO powder used in one CIP photodegradation cycle were examined. As shown by the XRD (Figure 2b) data, the structure-phase composition of the ZnO powder does not change. Figure 5 and Figure 6 show the overview spectra of ZnO powder and individual components Zn2P3/2 (a) and O1s (b) before and after photocatalysis. It can be seen that the spectral lines coincide. In addition, the compositions found according to XPS data (Table 2) coincide within the limits of the error of the measurement.

 doi:10.20944/preprints202310.0682.v1



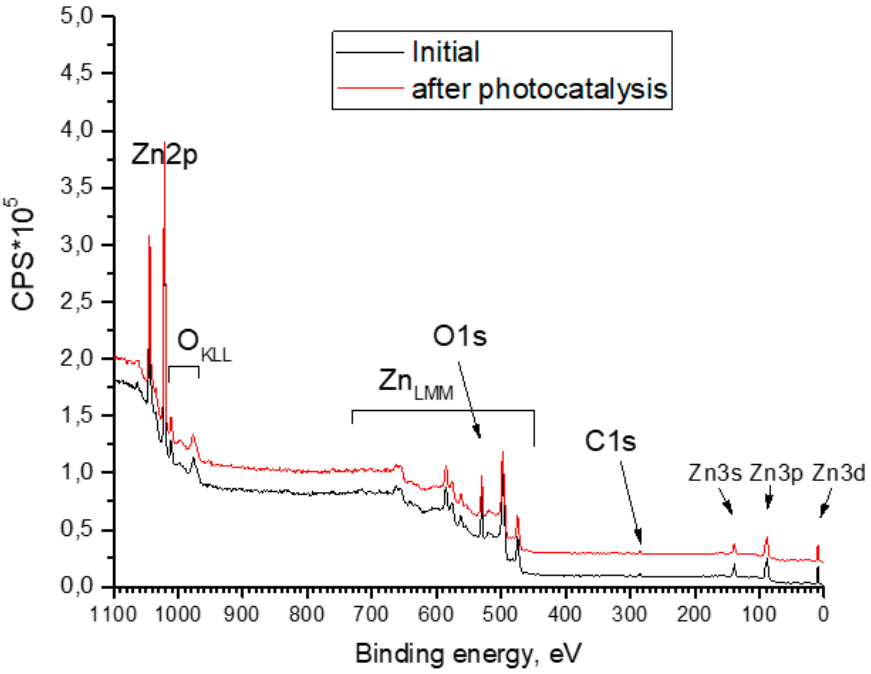


**Figure 5.** Panoramic XPS spectra of ZnO powder before and after photodegradation CIP.

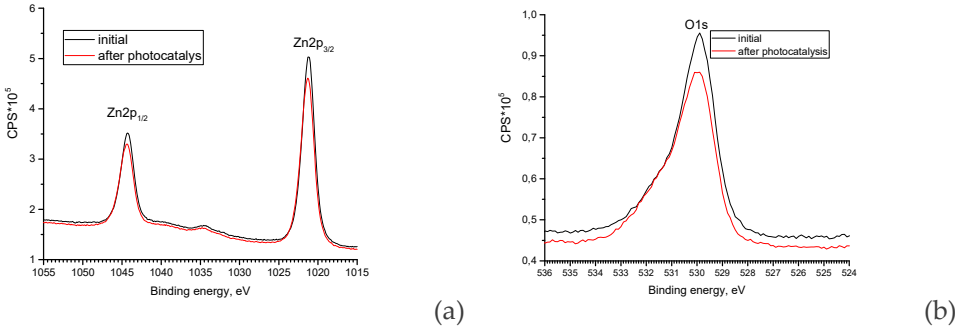


**Figure 6.** XPS spectra Zn2P$_{3/2}$ (**a**) and O1s (**b**).

Analysis of features in the XPS spectra before and after photocatalysis also demonstrates the presence of the same components: 530.1 eV (peak is characteristic of $O^{2-}$ ions of the surface lattice oxygen in ZnO matrix), 531.3 eV (attributed to oxygen defects in the matrix of metal oxides, related to oxygen vaccines), and 532.6 eV (band is related to surface hydroxyl (Zn—OH) group

## 4. Conclusions

The presented work studies the processes of synthesis of nitrogen-containing structures of ZnO using atmospheric pressure microwave nitrogen plasma and investigates their photocatalytic activity in the processes of degradation of 2,4-dinitrophenol and the antibiotic ciprofloxacin when irradiated with sunlight. The work proposes an effective plasma method for formation of photosensitive ZnO powders. Treatment of zinc metal powders using microwave nitrogen plasma has a number of advantages: a high gas temperature that promotes zinc evaporation and charging of microparticles with plasma particle streams (electrons and ions), preventing the formation of agglomerates. Both of these factors contribute to the formation of ZnO structures ranging in size from hundreds of nanometers to several micrometers. Study of the band gap parameters of ZnO structures using X-ray photoelectron spectroscopy demonstrates a high density of states near the Fermi level associated with defects contributing to the expansion of the photosensitivity range into the visible range. High

photoactivity was demonstrated (rate constants 0.036 min-1 and 0.051 min-1) of synthesized ZnO structures during photodegradation of 2,4-dinitrophenol and ciprofloxacin, respectively, when exposed to solar radiation. Photoactive structures of ZnO synthesized using microwave plasma can find application in processes of mineralization of toxic organic compounds.

**Author Contributions:** Conceptualization, A.M.,S.A., A.U., M.G.; methodology, A.M. and M.G.; validation, A.M. and M.G.; formal analysis, V.M.K.; investigation, S.A., A.U., A.M.; resources, A.M., M.G., S.A., A.U. and V.K.; writing, A.M.; writing—review and editing, A.M.; visualization, A.M.; supervision, A.M., M.G., and V.K.; project administration, A.M. and V.K.; funding acquisition, A.M. and V.K. All authors have read and agreed to the published version of the manuscript.

**Funding:** This research was performed in the frame of state assignments of the Ministry of Science and Higher Education of the Russian Federation for FSRC "Crystallography and Photonics" RAS, Federal State Budget Institution JIHT RAS.

**Data Availability Statement:** Not applicable.

**Acknowledgments:** The authors are grateful to R.G. Valeev (Center for Physical and Physico-Chemical Methods of Analysis, Study of the Properties and Characteristics of Surfaces, Nanostructures, Materials and Products, UdmFRC Ural Branch of the Russian Academy of Sciences) for their help in the study of samples by the method of XPS.

**Conflicts of Interest:** The authors declare no conflict of interest.

## References

1. Ren, G.; Han, H.; Wang, Y.; Liu, S.; Zhao, J.; Meng, X.; Li, Z. Recent Advances of Photocatalytic Application in Water Treatment: A Review. *Nanomaterials* **2021**, *11*, 1804. https://doi.org/10.3390/nano11071804.
2. Byrne, J.A.; Dunlop, P.S.M.; Hamilton, J.W.J.; Fernández-Ibáñez, P.; Polo-López, I.; Sharma, P.K.; Vennard, A.S.M. A Review of Heterogeneous Photocatalysis for Water and Surface Disinfection. *Molecules* **2015**, *20*, 5574–5615. https://doi.org/10.3390/molecules20045574.
3. Herrmann, J.-M. Heterogeneous photocatalysis: Fundamentals and applications to the removal of various types of aqueous pollutants . *Catalysis Today* **1999**, *53*, 115–129. https://doi.org/10.1016/s0920-5861(99)00107-8.
4. Matthews, R.W.; McEvoy, S.R. Destruction of phenol in water with sun, sand, and photocatalysis. *Solar Energy.* **1992**, *49*, 507–513. https://doi.org/10.1016/0038-092x(92)90159-8.
5. Mugumo, R.; Ichipi, E.; Tichapondwa, S.M.; Chirwa, E.M.N. Visible-Light-Induced Photocatalytic Degradation of Rhodamine B Dye Using a CuS/ZnS p-n Heterojunction Nanocomposite under Visible-Light Irradiation. *Catalysts* **2023**, *13*, 1184. https://doi.org/10.3390/catal13081184.
6. Chen, H.; Hu, Y.; Ying, Z.; Xia, Y.; Ye, J.; Zhao, J.; Zhang, S. BiOI-$SnO_2$ Heterojunction Design to Boost Visible-Light-Driven Photocatalytic NO Purification. *Int. J. Environ. Res. Public Health* **2023**, *20*, 4009.
7. Chowdhury, A.; Balu, S.; Lan, K.-W.; Wei-Chih Lee, L.; Yang, T.C.-K. Synergistic Effect of $BiVO_4$/P-g-$C_3N_4$ Heterojunction with Enhanced Optoelectronic Properties on Synthetic Colorants under Visible Light. *Colorants* **2023**, *2*, 426–442.
8. Yan, X.; Ning, G.; Zhao, P. Enhanced Visible Light Photocatalytic Reduction of Cr(VI) over a Novel Square Nanotube Poly (Triazine Imide)/$TiO_2$ Heterojunction. *Catalysts* **2019**, *9*, 55.
9. Wang, W.-Y.; Sang, T.; Zhong, Y.; Hu, C.-H.; Wang, D.-H.; Ye, J.-C.; Wei, N.-N.; Liu, H. Surfactant-Modified CdS/$CdCO_3$ Composite Photocatalyst Morphology Enhances Visible-Light-Driven Cr(VI) Reduction Performance. *Nanomaterials* **2022**, *12*, 3923. https://doi.org/10.3390/nano12213923.
10. Yadav, A.A.; Hunge, Y.M.; Kang, S.-W. Visible Light-Responsive $CeO_2$/$MoS_2$ Composite for Photocatalytic Hydrogen Production. *Catalysts* **2022**, *12*, 1185.
11. Mohamed, K.M.; Benitto, J.J.; Vijaya, J.J.; Bououdina, M. Recent Advances in ZnO-Based Nanostructures for the Photocatalytic Degradation of Hazardous, Non-Biodegradable Medicines. *Crystals* **2023**, *13*, 329.
12. Ma, S.; Huang, Y.; Hong, R.; Lu, X.; Li, J.; Zheng, Y. Enhancing Photocatalytic Activity of ZnO Nanoparticles in a Circulating Fluidized Bed with Plasma Jets. *Catalysts* **2021**, *11*, 77. https://doi.org/10.3390/catal11010077.
13. Alkauskas, A.; Pasquarello, A. Band-edge problem in the theoretical determination of defect energy levels: The O vacancy in ZnO as a benchmark case. *Physical Review B* **2011**, *84.* https://doi.org/10.1103/physrevb.84.125206.
14. Hanif, M.A.; Kim, Y.S.; Ameen, S.; Kim, H.G.; Kwac, L.K. Boosting the Visible Light Photocatalytic Activity of ZnO through the Incorporation of N-Doped for Wastewater Treatment. *Coatings* **2022**, *12*, 579. https://doi.org/10.3390/coatings12050579.

15. Heo, S.-G.; Jo, S.-I.; Jeong, G.-H. Revealing the enhanced photocatalytic properties of ZnO tetrapods produced by atmospheric-pressure microwave plasma jet system Current Applied Physics **2023**, *46*, 46–54. https://doi.org/10.1016/j.cap.2022.12.004.
16. Fortov, V.E.; Ivlev, A.V.; Khrapak, S.A.; Khrapak, A.G.; Morfill, G.E. Complex (dusty) plasmas: Current status, open issues, perspectives. *Phys. Rep.* **2005**, *421*, 1–103. https://doi.org/10.1016/j.physrep.2005.08.007.
17. Ishihara, O. Complex plasma: Dusts in plasma. *J. Phys. D Appl. Phys.* **2007**, *40*, R121.
18. Koohgard, M.; Masoudi Sarvestani, A.; Hosseini-Sarvari, M. Photocatalytic synthesis of unsymmetrical thiourea derivatives via visible-light irradiation using nitrogen-doped ZnO nanorods. *New J. Chem.* **2020**, *44*, 14505–14512. https://doi.org/10.1039/d0nj02197k.
19. Moisan, M.; Sauve, G.; Zakrzewski, Z.; Hubert, J. *Plasma Sources Sci. Technol.* **1994**, *3*, 584–592.
20. Baltin, L.; Batenin, V.M.; Lebedeva, V.; Tsemko, N.; Devyatkin, I. Stationary microwave discharge in nitrogen at atmospheric pressure. *High Temp.* **1971**, *9*, 1019.
21. Lavand, A.B.; Malghe, Y.S. Synthesis, characterization and visible light photocatalytic activity of nitrogen-doped zinc oxide nanospheres. *J. Asian Ceram. Soc.* **2015**, *3*, 305–310. https://doi.org/10.1016/j.jascer.2015.06.002.
22. García, J.F.; Sánchez, S.; Metz, R. Complete Oxidation of Zinc Powder. Validation of Kinetics Models. *Oxid. Met.* **2008**, *69*, 317–325. https://doi.org/10.1007/s11085-008-9099-9.
23. Hassan, N.; Jalil, A.; Fei, I.; Razak, M.; Khusnun, N.; Bahari, M.; Riwayati, Y.; Suprapto, S.; Prasetyoko, D.; Firmansyah, M.; et al. Vanadia as an electron-hole recombination inhibitor on fibrous silica-titania for selective hole oxidation of ciprofloxacin and Congo red photodegradation. *Chemosphere* **2023**, *338*, 139502. https://doi.org/10.1016/j.chemosphere.2023.139502.
24. Van Thuan, D.; Nguyen, T.B.; Pham, T.H.; Kim, J.; Chu, T.T.H.; Nguyen, M.V.; Nguyen, K.D.; Al-Onazi, W.A.; Elshikh, M.S. Photodegradation of ciprofloxacin antibiotic in water by using ZnO-doped g-C3N4 photocatalyst. *Chemosphere* **2022**, *308*, 136408. https://doi.org/10.1016/j.chemosphere.2022.136408.
25. Mukherjee, I.; Cilamkoti, V.; Dutta, R.K. Sunlight-Driven Photocatalytic Degradation of Ciprofloxacin by Carbon Dots Embedded in ZnO Nanostructures. *ACS Appl. Nano Mater.* **2021**, *4*, 7686–7697. https://doi.org/10.1021/acsanm.1c00883.
26. Costa, L.N.; Nobre, F.X.; Lobo, A.d.O.; de Matos, J.M.E. Photodegradation of ciprofloxacin using Z-scheme TiO2/SnO2 nanostructures as photocatalyst. *Environ. Nanotechnology, Monit. Manag.* **2021**, *16*, 100466. https://doi.org/10.1016/j.enmm.2021.100466.
27. Park, S.J.; Das, G.S.; Schütt, F.; Adelung, R.; Mishra, Y.K.; Tripathi, K.; Kim, T.M. Visible-light photocatalysis by carbon-nano-onion-functionalized ZnO tetrapods: Degradation of 2,4-dinitrophenol and a plant-model-based ecological assessment. *NPG Asia Mater.* **2019**, *11*, 8. https://doi.org/10.1038/s41427-019-0107-0.
28. Mao, L.; Shen, J.; Ma, X.; Lan, Z.; Zhang, X. Effects of operational parameters on the photodegradation of 2,4-dinitrophenol in TiO2dispersion. *Desalination Water Treat.* **2014**, *56*, 744–751. https://doi.org/10.1080/19443994.2014.937754.
29. Das, A.; S.K., N.; Nair, R.G. Influence of surface morphology on photocatalytic performance of zinc oxide: A review. *Nano-Struct. Nano-Objects* **2019**, *19*, 100353. https://doi.org/10.1016/j.nanoso.2019.100353.
30. Wang, M.; Zhang, Y.; Zhou, Y.; Yang, F.; Kim, E.J.; Hahn, S.H.; Seong, S.G. Rapid room-temperature synthesis of nanosheet-assembled ZnO mesocrystals with excellent photocatalytic activity. *CrystEngComm* **2013**, *15*, 754–763. *https://doi.org*/10.1039/c2ce26660a,.
31. Kislov, N.; Lahiri, J.; Verma, H.; Goswami, D.Y.; Stefanakos, E.; Batzill, M. Photocatalytic Degradation of Methyl Orange over Single Crystalline ZnO: Orientation Dependence of Photoactivity and Photostability of ZnO. *Langmuir* **2009**, *25*, 3310–3315. *https://doi.org*/10.1021/la803845f.
32. Vempati, S.; Mitra, J.; Dawson, P. One-step synthesis of ZnO nanosheets: A blue-white fluorophore. *Nanoscale Res. Lett.* **2012**, *7*, 470.
33. I. V. Rogozin, A.N. Georgobiani, M.B. Kotlyarevsky, and A. V. Marakhovskii, *Inorg. Mater.* **2009**, *45*, 391.